Linking Spatial Distributions of Potential and Current in Viscous Electronics

Gregory Falkovich[1,2] and Leonid Levitov[3]
[1]Weizmann Institute of Science, Rehovot 76100, Israel
[2]Institute for Information Transmission Problems, Moscow 127994, Russia
[3]Massachusetts Institute of Technology, Cambridge, Massachusetts 02139, USA
(Received 3 July 2016; published 10 August 2017)

Viscous electronics is an emerging field dealing with systems in which strongly interacting electrons behave as a fluid. Electron viscous flows are governed by a nonlocal current-field relation which renders the spatial patterns of the current and electric field strikingly dissimilar. Notably, driven by the viscous friction force from adjacent layers, current can flow against the electric field, generating negative resistance, vorticity, and vortices. Moreover, different current flows can result in identical potential distributions. This sets a new situation where inferring the electron flow pattern from the measured potentials presents a nontrivial problem. Using the inherent relation between these patterns through complex analysis, here we propose a method for extracting the current flows from potential distributions measured in the presence of a magnetic field.

DOI: 10.1103/PhysRevLett.119.066601

For electron transport in conductors, one can outline two broadly defined scenarios depending on the relative strength of disorder and interactions [1–4]. In the disorder-dominated regime one finds "individualist" behavior of electrons moving in straight lines like pinballs bouncing among impurities. Fast momentum relaxation gives the familiar Ohm's law with current locally proportional to the electric field. In the interaction-dominated regime, when particles exchange their momenta at the rates much faster than the disorder collision rates, electrons move in a neatly coordinated way, in many ways resembling the flow of viscous fluids [5–15]. The current-field relation changes drastically in this case [16].

Signatures of viscous flows have been observed in ultraclean GaAs, graphene, and $PdCoO_2$ [17–20]. Graphene, in particular, is well suited for studying electron viscosity since low disorder and weak electron-lattice coupling render momentum-conserving two-body (e-e) collisions dominant in a wide range of carrier densities and temperatures. In contrast, momentum-nonconserving umklapp e-e processes are forbidden because of graphene crystal symmetry. Gate-tunable and temperature-dependent collision rates help to realize the ballistic and viscous regime in a single sample.

Current in an electron fluid is locally proportional to momentum density, but its relation to the electric field is nonlocal since the viscous force is proportional to the velocity Laplacian. As a result, the electric field and current can be quite different vector fields. Unraveling the relation between them is one of the challenges of viscous electronics. In particular, one needs to find ways to reconstruct currents from the potentials, measurable by a variety of experimental techniques. As we will see, while the resulting integral relations are nontrivial, in two dimensions they can be tackled using a powerful framework of complex analysis. This provides a direct link between measured potentials and the current flow patterns.

We will see that the currents depend not only on the potentials but also, in an essential way, on the boundary conditions. As a result, identical potential distributions can correspond to *totally different flow patterns*. This surprising behavior is illustrated in Fig. 1 which shows a flow injected into a conducting half-plane through a pointlike source at the edge. For an incompressible flow, charge continuity yields $\nabla \cdot \mathbf{j} = ne\nabla \cdot \mathbf{v} = 0$. We resolve this condition by introducing the stream function

$$\mathbf{v} = \mathbf{z} \times \nabla\psi = (-\partial_y\psi, \partial_x\psi) \tag{1}$$

(see, e.g., Ref. [21]). The isolines of ψ define streamlines since their tangent is parallel to the velocity everywhere. Panels (a) and (b) in Fig. 1 present the streamlines for the no-stress (i.e., zero shear stress) and no-slip boundary conditions, respectively. In both cases the streamlines are straight lines pointing outward away from the source. However, the two flows have very different angular distributions, described by the stream functions

$$\psi_1(\theta) = \frac{\tilde{I}}{4\pi}(\sin 2\theta - 4\theta), \quad \psi_2(\theta) = \frac{\tilde{I}}{2\pi}(\sin 2\theta - 2\theta), \tag{2}$$

where $\theta = \tan^{-1} y/x$ is the polar angle and $\tilde{I} = I/ne$ is current nondimensionalized with the carrier density and charge. The currents depend on the angle, respectively, as $1 + \sin^2\theta$ and $2\sin^2\theta$. The potential map is identical in both cases, taking negative values at the boundary [16,18,22], see Eq. (11) and discussion below. Both flows pictured in Fig. 1 have nonzero vorticity $\omega(\mathbf{r}) = \nabla \times \mathbf{v}$; however the streamlines do not form loops. This illustrates that, in a departure from a common belief, vortices are not required for negative voltage to occur.

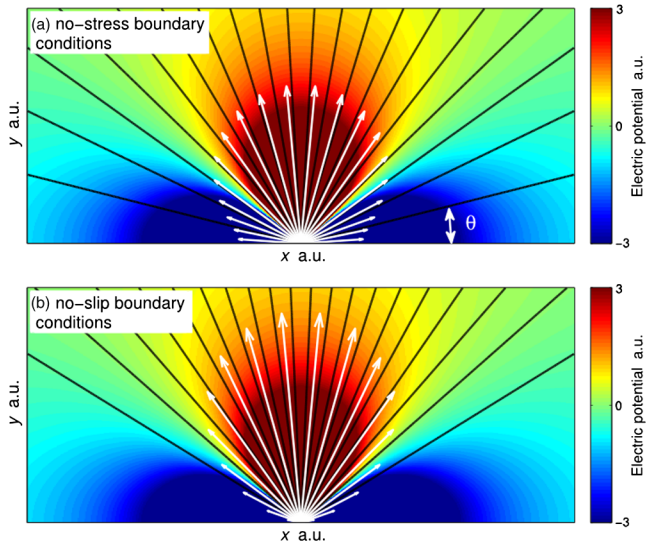

FIG. 1. Streamlines (black) and potential color map for current injected through a point in a half-plane, Eqs. (2) and (11). The velocity is shown by white arrows, its magnitude is proportional to the density of streamlines. Boundary conditions: (a) no stress (i.e., shear-stress free); (b) no slip.

Understanding the current and voltage distributions in two dimensions is facilitated by complex analysis which organizes distinct physical fields into a single holomorphic function. On the account of long-range Coulomb interactions, we treat electrons as an incompressible fluid. A low-Reynolds flow obeys the Stokes equation which states the balance of viscous friction and electric force:

$$\eta\nabla^2\mathbf{v}(\mathbf{r}) = ne\nabla\phi(\mathbf{r}). \tag{3}$$

Here $\phi(\mathbf{r})$ is the electric potential and η is the viscosity. Combining Eqs. (3) and (1), we see that the vorticity $\omega = \nabla^2\psi = (\partial_x^2 + \partial_y^2)\psi$ and ϕ form a Cauchy-Riemann pair

$$\partial_x\omega = (en/\eta)\partial_y\phi, \qquad \partial_y\omega = -(en/\eta)\partial_x\phi. \tag{4}$$

The quantities ω and ϕ are therefore proportional to the imaginary and real part of a holomorphic function of $z = x + iy$, respectively. This behavior is distinct from the Ohmic case $\mathbf{j} = en\mathbf{v} = -\sigma\nabla\phi$, where

$$en\mathbf{z}\times\nabla\psi = -\sigma\nabla\phi. \tag{5}$$

In this case it is the stream function ψ that takes on the role of a Cauchy-Riemann counterpart of the potential ϕ.

Before moving on, we discuss the validity of Eq. (3). In a clean conductor, such as graphene, Eq. (3) holds at the length scales greater than the e-e collision mean free path ℓ_{ee} but shorter than the length scales set by momentum-nonconserving scattering by residual disorder or phonons. The latter can be described by a resistivity term as

$$(\eta\nabla^2 - n^2e^2\rho)\mathbf{v}(\mathbf{r}) = ne\nabla\phi(\mathbf{r}). \tag{6}$$

The new term, despite being small, becomes relevant at distances exceeding $\ell_* = \sqrt{\eta/n^2e^2\rho}$. To estimate ℓ_* we use the Drude model for resistivity, $\rho = p_F/ne^2\ell_p$ with ℓ_p the elastic mean free path, and express the dynamic viscosity as $\eta = nm\nu$. Here the kinematic viscosity ν represents the momentum diffusion coefficient, $\nu \sim v\ell_{ee}$. Combining these estimates we arrive at $\ell_* = (\ell_p\ell_{ee})^{1/2}$. In a clean system, e.g., graphene, these length scales satisfy $\ell_{ee} \ll \ell_* \ll \ell_p$. The values ℓ_p and ℓ_{ee}, estimated for graphene [23], yield ℓ_* on the order of a few micrometers. Below we focus on the length scales $\ell_{ee} \ll r \ll \ell_*$ where Eq. (3) holds. Detailed analysis of both viscous and Ohmic effects through Eq. (6) can be found in Ref. [23].

Extracting the current spatial dependence from that for the potential, which is readily measurable by a variety of experimental techniques [26,27], can in principle be done by inverting the integral relations [Eq. (4)]. However, instead of facing this hard task, here we suggest an approach that involves direct measurements rather than indirect computations (cf. Ref. [28]). Namely, we propose measuring magnetoresistance in the presence of a classically weak magnetic field, such that the cyclotron radius is much greater than the mean free path ℓ_{ee}. In this case, the Eqs. (3) and (6) acquire an extra term due to the Lorentz force: $(\eta\nabla^2 - n^2e^2\rho)\mathbf{v} = ne\nabla\phi + neB\mathbf{v}\times\mathbf{z}$. Substituting Eq. (1) we obtain

$$(\eta\nabla^2 - n^2e^2\rho)\mathbf{v}(\mathbf{r}) = ne\nabla\phi(\mathbf{r}) + neB\nabla\psi. \tag{7}$$

Taking the curl of Eq. (7) we obtain $[\eta(\nabla^2)^2 - n^2e^2\rho\nabla^2]\psi = ne(\mathbf{v}\cdot\nabla)B$. We see that when the magnetic field does not change along the flow, the stream function ψ obeys the equation identical to that at $B = 0$.

Writing Eq. (7) as a balance between momentum loss due to the Ohmic term and the divergence of the momentum flux, we see that constant B enters only the diagonal (pressure) part of the flux:

$$\frac{\partial}{\partial x_i}\left[ne(\phi + B\psi)\delta_{ik} + \eta\left(\frac{\partial v_i}{\partial x_k} + \frac{\partial v_k}{\partial x_i}\right)\right] = \rho n^2e^2v_k. \tag{8}$$

Equation (8) implies that the constant magnetic field does not affect the boundary conditions on ψ considered here. Indeed, the tangential derivative of ψ is completely determined by the incoming or outgoing current. The normal derivative (equal to the tangential velocity) is determined by friction, that is by the continuity across the boundary of the normal flux of tangential momentum $p_\parallel$, i.e., the off-diagonal part of the flux tensor in Eq. (8). The no-slip condition (zero $p_\parallel$) means full momentum relaxation at the boundary, which apparently cannot be affected by the magnetic field. The no-stress condition (zero flux of $p_\parallel$)

takes place when fluid borders the medium which does not support tangential stress; here again the magnetic field does not change the condition. The same is true for the mixed boundary condition, where the flux of tangential momentum at the system boundary is proportional to the tangential velocity [23].

Since neither equation nor boundary conditions change, we conclude that the stream function remains unchanged when a constant weak B field is applied. Under these conditions, the quantity $\phi + B\psi$ must be equal to the potential obtained at $B = 0$. Therefore, the ϕ and ψ dependence on B takes on a very simple form

$$\phi_{B\neq 0}(\mathbf{r}) = \phi_0(\mathbf{r}) - B\psi_0(\mathbf{r}), \qquad \psi_{B\neq 0}(\mathbf{r}) = \psi_0(\mathbf{r}), \tag{9}$$

where the subscript zero denotes the quantities found at $B = 0$. This relation can be used to obtain the stream function ψ directly from the electric potential measurements. Alternatively, and perhaps more conveniently, ψ can be obtained through antisymmetrization as

$$2B\psi_0(\mathbf{r}) = \phi_{-B}(\mathbf{r}) - \phi_B(\mathbf{r}). \tag{10}$$

The stream function is a fundamental fluid-mechanic quantity that describes incompressible flows. The relation Eq. (10) therefore provides a vehicle that directly relates current flows with the measured potentials. Repeating the steps that have led us to Eq. (4), we see that for viscous flow in the presence of a B field, the Cauchy-Riemann relations are obeyed by the quantities ω and $\phi + B\psi$.

As one can see from Eq. (4), the electric field can only arise in the presence of nonuniform flow vorticity. To better understand the role of vorticity, we recall that viscous friction is determined by the symmetric part of the tensor of velocity derivatives. The vorticity, which is the antisymmetric part of this tensor, describes rotation of a fluid element as a whole that does not cause friction (e.g., see Ref. [21]). It is vorticity *inhomogeneity* that produces the electric field required to balance viscous friction. The relations Eq. (4) imply, in particular, that in irrotational viscous flows, wherein $\omega = 0$, the electric potential ϕ is constant and the electric force vanishes in the bulk. Such "freely flowing" currents are described by a velocity potential, $\mathbf{v} \propto \nabla\lambda$. Potential flows occur when the vorticity vanishes on the boundaries, in which case it can be shown to vanish everywhere. In terms of the electric potential ϕ this translates into equipotential, i.e., metallic boundaries (the fascinating topic of electric field expulsion from viscous charge flows with metallic boundaries will be discussed elsewhere). In contrast, the potential is not identically constant and the vorticity is nonzero for nonmetallic boundaries, in which case a wide variety of nontrivial current and potential patterns can arise.

An instructive example is provided by viscous flows originating from a point source at the edge of the half-plane $y \geq 0$. The solution for general boundary conditions including no slip and no stress as limiting cases is presented in Ref. [23]. For the no-stress limit it gives Eq. (2). The vorticity can then be derived as $\omega = \nabla^2\psi = \tilde{I}\mathrm{Im}\, z^{-2}/2$. The potential, obtained from Eq. (4), has a quadrupole form:

$$\phi(x,y) = \frac{\tilde{I}\eta}{2ne}\mathrm{Re}\; z^{-2} = -\frac{\tilde{I}\eta}{2ne}\frac{\cos 2\theta}{r^2}. \tag{11}$$

In the no-slip case, in a similar vein, we find $\psi_2(\theta)$ in Eq. (2). Interestingly, while the streamlines are straight lines directed outward from the source in both cases, the actual velocity patterns are quite different (see Fig. 1). The quantities ω and ϕ, obtained from $\psi_2(\theta)$, have the same form as in Eq. (11) but are twice larger than in the no-stress case, where there is no edge friction.

Both the viscous force and the electric force, balancing each other, are nonzero. The electric field exhibits multiple sign changes,

$$\frac{\partial\phi}{\partial r} \propto \frac{\cos 2\theta}{r^3}, \qquad r^{-1}\frac{\partial\phi}{\partial\theta} \propto \frac{\sin 2\theta}{r^3}, \tag{12}$$

reflecting that the electric forces push the fluid outward for $\pi/4 < \theta < 3\pi/4$ but pull it inward near boundaries, where they balance the viscous drag from the faster-moving adjacent layers of the fluid. It is this field that produces the negative voltage at the edge [16].

Having established that vorticity is necessary for the appearance of the electric field inside a viscous charge flow, we now discuss vortices. It is important to distinguish the generic features due to local vorticity from a more specific global pattern of a vortex. Indeed, nonzero vorticity at a point means that an infinitesimal fluid element rotates as it moves. Such motion, however, may take place even along perfectly straight streamlines such as those in the flows pictured in Fig. 1, where vorticity is nonzero since different streamlines have different velocities. Vortices, on the other hand, are defined by closed-loop streamlines, that is they are global rather than local structures. Accordingly, unlike the half-plane geometry in Fig. 1, vortices can be readily produced in a confined geometry. Vortices can be characterized by *separatrix* lines which separate the closed and open streamlines. Below we illustrate this general behavior for a strip of a finite width.

We start with the no-stress boundary condition and consider the pointlike source and drain positioned at (0,0) and $(0,w)$ in the strip $-\infty < x < \infty$, $0 < y < w$. A solution of the biharmonic equation with $\partial_x\psi = \tilde{I}\delta(x)$ and $\partial^2\psi/\partial y^2 = 0$ at $y = 0, w$ reads

$$\psi(x,y) = \frac{\tilde{I}}{4\pi}\int_{-\infty}^{\infty}\frac{e^{ikx}dk}{ik\cosh\frac{kw}{2}}(a\cosh k\tilde{y} - k\tilde{y}\sinh k\tilde{y}), \tag{13}$$

where we defined $\tilde{y} = y - w/2$ and $a = 2 + (kw/2)\tanh(kw/2)$. The streamlines, given by the contours of

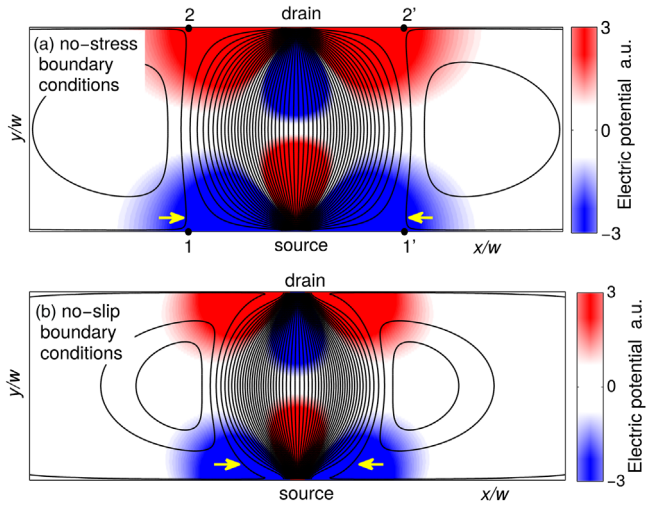

FIG. 2. Current streamlines (black) and potential color map for a flow across the strip. Arrows mark the streamlines nearest to separatrices. Stagnation points are labeled $s_{1,2}$, $s'_{1,2}$. To elucidate the behavior near contacts, two regions are shown with a tenfold density of streamlines. Boundary conditions: (a) no stress, (b) no slip.

ψ, are pictured in Fig. 2(a). The flow, directed from source to drain along the nominal current path, mimics that in Fig. 1 near each contact. Closed streamlines form a pair of vortices.

To analyze the separatrices of the flow, we consider the velocity at the boundary $y = 0$. Simple algebra yields

$$v_x(x,0) = -\frac{\partial\psi}{\partial y} = \frac{I(2 - \frac{\pi x}{w}\coth\frac{\pi x}{w})}{4wne\sinh(\pi x/w)}. \quad (14)$$

At $|x| \ll w$, the velocity is directed away from the source as in a half-plane, $v_x \propto 1/x$. However, v_x is directed *towards* the source at $|x| \gg w$, representing backflow due to vortices. We therefore conclude that there are stagnation points at the edge, where $v_x = v_y = 0$. At such points, marked s_1, s_2, s'_1, s'_2 in Fig. 2(a), two streamlines meet: one directed along the strip edge and another perpendicular to it. The latter represents a separatrix between the source-to-drain streamlines and the vortex streamlines. The stagnation points are defined by the equation $\pi x/w = 2\tanh(\pi x/w)$, giving $x/w = \pm 0.61$. This is in accord with the flow shown in Fig. 2(a), where arrows mark the streamlines nearest to the separatrices.

The potential is obtained by solving Eq. (3) which gives

$$\phi(x,y) = \alpha\int_{-\infty}^{\infty} dk e^{ikx}\frac{k\sinh k\tilde{y}}{\cosh\frac{kw}{2}} = \frac{\alpha\pi^2}{w^2}\mathrm{Re}\frac{\cosh\pi z}{\sinh^2\pi z}, \quad (15)$$

where $\alpha = I\eta/\pi(ne)^2$ and $z = (x+iy)/w$. Amusingly, this result can also be obtained from the solution for the source and drain in the half-plane, $\phi(z') = \mathrm{Re}[(z'-1)^{-2} - (z'+1)^{-2}]$, by mapping it onto the strip. Both the potential and the flow, taken near each contact, mimic those found for a point source in the half-plane.

The topology of the flow can change drastically upon altering the boundary conditions. As we now show, the flow found for the no-stress case undergoes a global change upon switching to the no-slip boundary conditions. This behavior is a manifestation of the fundamental nonlocality of viscous flows discussed above. The stream function for the no-slip case is of the form [16]

$$\psi(x,y) = \frac{\tilde{I}}{2\pi}\int_{-\infty}^{\infty}\frac{dk}{ik}e^{ikx}\frac{c_1\cosh k\tilde{y} - c_2 k\tilde{y}\sinh k\tilde{y}}{kw + \sinh kw}, \quad (16)$$

where $c_1 = kw\cosh(kw/2) + 2\sinh(kw/2)$, $c_2 = 2\sinh(kw/2)$. From Fig. 2(b) it may appear that the streamlines form radial patterns near contacts identical to those in Fig. 2(a), with $-\tilde{I}/2 < \psi < \tilde{I}/2$. However, a closer inspection reveals additional streamlines corresponding to the boundary values $\psi = \pm\tilde{I}/2$. These streamlines leave the contacts horizontally and then curve inward. Their form can be obtained explicitly by evaluating ψ in the domain $y \ll x \ll w$. Treating kw as a large parameter, we write

$$\pi\psi(x,y)/\tilde{I} \approx \arctan(x/y) + xy/(x^2+y^2) + 2xy/w^2 \approx \pi/2 - 2y^3/3x^3 + 3xy^2/w^3. \quad (17)$$

The terms first-order in y cancel, which allows for a second streamline with the same ψ value as at the edge, $\psi(x,y) = \tilde{I}/2$. This line, described by $y = 9x^4/2w^3$ at small y, is a separatrix between the source-to-drain streamlines and the vortex streamlines. This is illustrated in Fig. 2(b) where arrows mark the streamlines nearest to the separatrices. The vortex streamlines fill the space between the separatrix and the strip edge, extending arbitrarily close to the contacts.

To confirm that the streamlines below the separatrix turn around without reaching the source, we analyze the velocity $v_x = -\partial\psi/\partial y$. For $y \ll x \ll w$, approximating

$$\int_0^{\infty}\frac{k}{2}dk\sin kx(ye^{-ky} - w\sinh kye^{-kw}) \approx \frac{y^2}{x^3} - \frac{xy}{w^3}, \quad (18)$$

we see that the horizontal velocity reverses its sign at the "demarcation" line $y = x^4/w^3$ (lying below the separatrix) which means that upon crossing this line the streamlines turn around. Below this line, the second term in Eq. (18) dominates, making the flow along the edge directed towards the contact. In the limit $w \to \infty$, when the strip turns into a half-plane, the demarcation line disappears. In this case there are no closed streamlines and no backflow.

The qualitative difference between the no-slip and no-stress boundary conditions is manifested in the different dependence of the flows on the sample shape. If we replace the infinite strip by a rectangle $0 < y < w$, $-L < x < L$,

then the stagnation points and separatrices disappear in the no-stress case for the sufficiently small aspect ratio L/w. However, in the no-slip case, the separatrices survive and the vortices persist at any aspect ratio [23].

Potential distribution, obtained from Eq. (3), looks similar in both cases and does not reflect the presence of the separatrices and backflow, see Fig. 2(b). It changes sign twice on the nodal lines that make the angles $\pm\pi/4$ with the edge, as in a half-plane. We conclude that, while there is always a backflow along the edges in a wide strip, $L \gg w$, this backflow (while interesting in itself) is of little relevance for the negative voltage measured in Ref. [18]. Likewise, the voltage singularities near the contacts reflect diverging streamlines and have nothing to do with the vortices or separatrices (see Fig. 1).

In summary, we demonstrated that it is the negative electric field rather than a backflow that is a true universal signature of viscous electron transport. While the negative field is inherently related to the vorticity of current flow, it requires neither backflow nor vortices. Further, there is no one-to-one relation between the spatial distributions of currents and potentials, making it nontrivial to infer the current flow from the measured potential. Answer is provided by application of a weak magnetic field, which effects a change in the potential distribution proportional to the current stream function. This opens the door to direct measurements of viscous electron flow patterns by the well-developed charge and potential sensing techniques [26,27].

We acknowledge support of the Center for Integrated Quantum Materials (CIQM) under NSF Grant No. 1231319 (L. L.), partial support by the U.S. Army Research Laboratory and the U.S. Army Research Office through the Institute for Soldier Nanotechnologies, under Contract No. W911NF-13-D-0001 (L. L.), MISTI MIT-Israel Seed Fund (L. L. and G. F.), the Israeli Science Foundation (Grant No. 882) (G. F.) and the Russian Science Foundation (Project No. 14-22-00259) (G. F.).

[1] R. N. Gurzhi, Usp. Fiz. Nauk **94**, 689 (1968)[Sov. Phys. Usp. **11**, 255 (1968)].
[2] E. M. Lifshitz and L. P. Pitaevskii, *Physical Kinetics* (Pergamon Press, New York, 1981).
[3] R. Jaggi, J. Appl. Phys. **69**, 816 (1991).
[4] K. Damle and S. Sachdev, Phys. Rev. B **56**, 8714 (1997).
[5] M. Müller, J. Schmalian, and L. Fritz, Phys. Rev. Lett. **103**, 025301 (2009).
[6] M. Mendoza, H. J. Herrmann, and S. Succi, Phys. Rev. Lett. **106**, 156601 (2011).
[7] A. V. Andreev, S. A. Kivelson, and B. Spivak, Phys. Rev. Lett. **106**, 256804 (2011).
[8] D. Forcella, J. Zaanen, D. Valentinis, and D. van der Marel, Phys. Rev. B **90**, 035143 (2014).
[9] A. Tomadin, G. Vignale, and M. Polini, Phys. Rev. Lett. **113**, 235901 (2014).
[10] D. E. Sheehy and J. Schmalian, Phys. Rev. Lett. **99**, 226803 (2007).
[11] L. Fritz, J. Schmalian, M. Müller, and S. Sachdev, Phys. Rev. B **78**, 085416 (2008).
[12] B. N. Narozhny, I. V. Gornyi, M. Titov, M. Schütt, and A. D. Mirlin, Phys. Rev. B **91**, 035414 (2015).
[13] A. Principi, G. Vignale, M. Carrega, and M. Polini, Phys. Rev. B **93**, 125410 (2016).
[14] A. Cortijo, Y. Ferreirós, K. Landsteiner, and M. A. H. Vozmediano, Phys. Rev. Lett. **115**, 177202 (2015).
[15] A. Lucas, J. Crossno, K. C. Fong, P. Kim, and S. Sachdev, Phys. Rev. B **93**, 075426 (2016).
[16] L. Levitov and G. Falkovich, Nat. Phys. **12**, 672 (2016).
[17] M. J. M. de Jong and L. W. Molenkamp, Phys. Rev. B **51**, 13389 (1995).
[18] D. A. Bandurin *et al.*, Science **351**, 1055 (2016).
[19] J. Crossno *et al.*, Science **351**, 1058 (2016).
[20] P. J. W. Moll, P. Kushwaha, N. Nandi, B. Schmidt, and A. P. Mackenzie, Science **351**, 1061 (2016).
[21] G. Falkovich, *Fluid Mechanics, A Short Course for Physicists* (Cambridge University Press, Cambridge, England, 2011).
[22] I. Torre, A. Tomadin, A. K. Geim, and M. Polini, Phys. Rev. B **92**, 165433 (2015).
[23] See Supplemental Material at http://link.aps.org/supplemental/10.1103/PhysRevLett.119.066601 for an estimate of the crosssover length scale from viscous to Ohmic regime, and for analysis of viscous flow in the half-plane and rectangle geometries, which includes Refs. [24,25].
[24] A. B. Kashuba, Phys. Rev. B **78**, 085415 (2008).
[25] T. Taychatanapat, K. Watanabe, T. Taniguchi, and P. Jarillo-Herrero, Nat. Phys. **9**, 225 (2013).
[26] M. J. Yoo *et al.*, Science **276**, 579 (1997).
[27] A. Yacoby, H. F. Hess, T. A. Fulton, L. N. Pfeiffer, and K. W. West, Solid State Commun. **111**, 1 (1999).
[28] M. Beria, Y. Iqbal, M. Di Ventra, and M. Müller, Phys. Rev. A **88**, 043611 (2013).